Research in Astronomy and Astrophysics, 23:065001 (11pp), 2023 June https://doi.org/10.1088/1674-4527/acc91a

Effect of Orbital Characteristic of Inclined Third-body on Motion of Secondary-body for a Hierarchical Triple Systems

Majid Bakhtiari
Assistant Professor, School of Advanced Technologies, Iran University of Science and Technology, Narmak, Tehran 16844, Iran; bakhtiari_m@iust.ac.ir
Received 2022 August 19; revised 2022 November 3; accepted 2022 November 16; published 2023 May 10

Abstract

The influence of a third-body's orbital elements on the second-body's motion in a hierarchical triple system is a crucial problem in astrophysics. Most prolonged evaluation studies have focused on a distant zero-inclined third-body. This study presents a new perspective on second-body motion equations that addresses a perturbing-body in an elliptic orbit derived with consideration of the axial-tilt (obliquity) of the primary. The proposed model is compared by the dual-averaged method and the *N*-body problem algorithm. After validation, a generalized three-body model is derived to investigate the effects of the third-body's orbital elements on secondary-body motion behavior. The proposed model considers short-time oscillations that affect secular evaluation and applies to exoplanets with all the primary and third body eccentricities, inclinations, and mass ratios. It is shown that the obliquity of the primary (or third-body's inclination) must be considered for precise long-term assessment, even in highly-hierarchical systems.

Key words: celestial mechanics – planets and satellites: dynamical evolution and stability – Planetary Systems – gravitation

1. Introduction

The disturbing effect of a third-body on a secondary-body's motion in a hierarchical triple system is a crucial problem in astrophysics. It has wide applications in star systems and exoplanets (Han et al. 2014; Ricker et al. 2015), and has been extensively studied in the literature (Domingos et al. 2014, 2015; Nie & Gurfil 2021). There are evaluations of the orbital elements of a secondary-body that orbits around a primary-body on a timescale of thousands of days; hence, it would be impossible to plan such evaluations without addressing third-body orbit characteristics (Bakhtiari et al. 2017b). In prior studies, the *X*-*Y* plane of the inertial coordinate (placed on the centroid of the primary-body) has been used as the third-body orbital plane for simplification instead of relying on the primary-body's equatorial plane (Carvalho et al. 2011; Sosnitskii 2014; Rollin et al. 2016; Lara 2022) and the restricted three-body problem (Wang et al. 2016; Abouelmagd et al. 2020; Abbasali et al. 2021; Saeed & Zotos 2021). It means that the obliquity (axial-tilt) of the primary-body is ignored, and the equatorial plane of the primary-body is assumed to be the perturbing-body orbital plane. This simplification may lead to significant error in long-term evaluations of a three-body problem, especially for exoplanets that orbit on inclined orbits. The star 30 Arietis B is one of the stellar companions for which consideration of orbital inclination became important due to the effect on the system's stability (Kane et al. 2015). This issue is due to the existence of a relatively large separation of the detected stellar companion to 30 Arietis B. Further, the evaluation of inclination is important in such a system. In most previous works, the disturbing function (model for third-body perturbation) is expanded in the form of Legendre polynomials truncated up to the second-order term (quadrupole term) and a single-average (averaged over the secondary-body orbit) or double-average (averaged over the third-body orbit plus averaged over the secondary-body orbit) model is employed without consideration of the primary-body's obliquity (Bello & Singh 2015; Gomes & de Cássia Domingos 2016; Neishtadt et al. 2018, 2021). Single- and dual-average methods are used to eliminate short-period terms by decreasing the degrees of freedom of the motion equations of the secondary-body. Besides neglecting obliquity, the single-average model becomes inefficient when considering the primary-body's oblateness or other perturbations (Grishin et al. 2017). Therefore, the primary-body is neglected in previous works in favor of the single-average technique. Also, the double-average process does not consider short-term effects that affect the secular evolution and break down when conducting long-term evaluation. This error is more striking for a moderately-hierarchical three-body system because the disturbing force's short-time oscillation and high-order expansion (Ito 2016) are ignored (Katz et al. 2011).

A non-simplified model is proposed in this paper to overcome the accumulated error in prolonged evaluation of this problem in previous works caused by neglect of axial-tilt, the breakdown of the dual-averaged (DA) approximation over the long-term or a highly-eccentric orbit, and inaccuracy due to expansion of the third-body potential to a quadrupole term in a moderately-hierarchical system (Luo et al. 2016). This study has developed a non-simplified secondary-body motion model by considering third-body gravity and investigating the prolonged effects of primary-body obliquity. The proposed model is valid for long-term evaluations of a moderately-hierarchical and massive third-body system. In addition, it will be shown that the DA model will be inaccurate and inapplicable when the disturbing-body is massive in a moderately-hierarchical system. This paper illustrates the effect of obliquity on the variation of a prolonged orbital element and critical inclination. It is shown that obliquity should be considered for a planet on an inclined or eccentric orbit, like some exoplanetary systems. This aspect is demonstrated in several generalized three-body system simulations. This study is organized as follows: Section 2 proposes a non-simplified model of an oblate primary-body orbiter considering the inclined-elliptical third-bodies for prolonged investigation. The proposed model can assess short-term variations and avoid error accumulation in the long-term evaluation of prior models such as the DA model (Liu et al. 2012; Luo et al. 2016). Section 3 provides numerical results to validate the proposed model and demonstrate the importance of obliquity and the non-simplified model. Also, the effect of orbital elements of a third-body is investigated on the secondary-body motion in a generalized moderately-hierarchical three-body system. An inclined, eccentric, massive third-body is applied to the proposed model with obliquity to demonstrate the imperfections in the DA model. Finally, Section 4 summarizes the results and presents the conclusion and reasons for this research.

2. The Dynamic Model

The system explained in this investigation includes an inner binary of two celestial bodies (a primary- and secondary-body with mass M and m, respectively), and a perturbing-body with mass m_3. The changes in outer orbit (third-body orbit) are neglected, and the outer orbit is assumed to be Keplerian. The system's geometry is illustrated in Figure 1 as an attractive physical case of $m_3 \geqslant M \gg m$ (the test particle limit). Also, the coordinate system ($OXYZ$) describes the inertial frame whose origin is attached to the primary-body's center of mass. The $X-Y$ plane concurs with the primary-body's equatorial plane, and the north pole of the primary-body is supposed to be along the Z-axis (Bakhtiari et al. 2017c).

The angular rotational velocity of the Local Vertical-Local Horizontal (LVLH) coordinate is

$$\boldsymbol{\omega} = \omega_x \boldsymbol{x} + \omega_y \boldsymbol{y} + \omega_z \boldsymbol{z}, \tag{1}$$

where ω_x and ω_z are the steering and orbital rate of the secondary-body's orbital plane, respectively. According to the

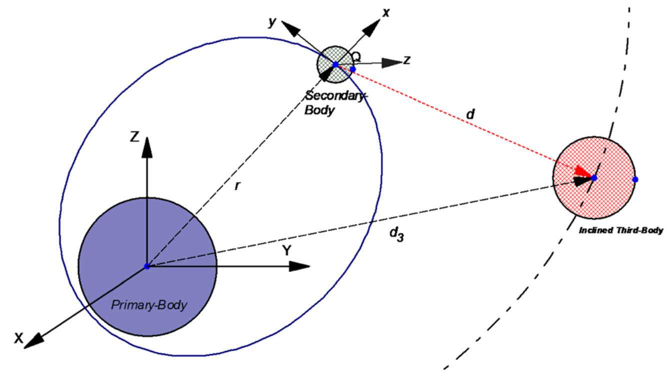

Figure 1. The configuration of the primary- and secondary-body as the inner two celestial objects in the presence of an inclined perturbing-body.

orbital elements of the secondary-body, ω_x and ω_z are written as (Xu & Wang 2008)

$$\omega_x = \cos(\theta)\frac{di}{dt} + \sin(\theta)\cos(i)\frac{d\Omega}{dt}, \tag{2}$$

$$\omega_z = \frac{d\theta}{dt} + \cos(i)\frac{d\Omega}{dt}, \tag{3}$$

where s_* and c_* represent $\sin(*)$ and $\cos(*)$ respectively. Moreover, i, θ, Ω render inclination, the argument of latitude, and the right ascension of ascending node (RAAN), respectively. The derivatives of the unit vectors are yielded as

$$\frac{d}{dt}(x) = \boldsymbol{\omega} \times \boldsymbol{x} = \omega_z \boldsymbol{y}, \tag{4}$$

$$\frac{d}{dt}(y) = \boldsymbol{\omega} \times \boldsymbol{y} = \omega_x \boldsymbol{z} - \omega_z \boldsymbol{x}, \tag{5}$$

$$\frac{d}{dt}(z) = \boldsymbol{\omega} \times \boldsymbol{z} = -\omega_x \boldsymbol{y}, \tag{6}$$

$$x = \frac{\boldsymbol{r}}{|r|},\ z = \frac{\boldsymbol{h}}{|h|},\ \boldsymbol{y} = \boldsymbol{z} \times \boldsymbol{x}, \tag{7}$$

where $h = |\boldsymbol{r} \times \dot{\boldsymbol{r}}|$ is the angular momentum. Also, the angular velocity component of the y-axis equals zero (Kechichian 1998).

$$\omega_y = -\sin(\theta)\frac{di}{dt} + \cos(\theta)\sin(i)\frac{\Omega}{dt} = 0. \tag{8}$$

2.1. Secondary-body Motion Affected by Inclined Third-body

The secondary-body motion is described by hybrid orbital elements (r, v_x, i, h, θ, Ω) (Bakhtiari et al. 2017c) Also, the third-body is in an inclined orbit with semimajor axis a_3, eccentricity e_3, argument of perigee ω_3, argument of latitude θ_3, and RAAN Ω_3 (Xu et al. 2012). Also, the potential function of the system is stated as (Bakhtiari et al. 2017a)

$$W_3 = \mu_3\left(\frac{1}{d_3} - \frac{1}{{r'_n}^3}\boldsymbol{r}\cdot r_3\right), \tag{9}$$

where μ_3 is the gravitational constant of the third-body, $r_3 = x_3\boldsymbol{x} + y_3\boldsymbol{y} + z_3\boldsymbol{z}$ is the vector that adjoins the centers of the primary-body and third-body in the LVLH frame, and $\boldsymbol{d_3} = \boldsymbol{r_3} - \boldsymbol{r}$ is the vector from the secondary-body to the third-body center, expressed as

$$d_3 = \sqrt{(x_3 - r)^2 + {y_3}^2 + {z_3}^2}. \tag{10}$$

The gradient of the potential function of the perturbing-body is set as follows

$$\nabla W_3 = \mu_3\left(\frac{1}{r_3^3} - \frac{1}{d_3^3}\right)\boldsymbol{r}_3 - \frac{\mu_3}{d_3^3}\boldsymbol{r}. \tag{11}$$

Additionally, the gradient of the primary-body's gravitational potential function must be present in the LVLH frame. The potential gravitational function of the oblate primary-body can be derived as below (Bakhtiari et al. 2017c)

$$\begin{aligned} U &= -\tfrac{\mu}{r} - \tfrac{k_{J2}}{r^3}\left(\tfrac{1}{3} - \sin^2(i)\sin^2(\theta)\right),\\ k_{J2} &= 3J_2\mu R_e^2/2. \end{aligned} \tag{12}$$

The gradient of the gravitational potential of the primary-body is derived in the LVLH frame as

$$\begin{aligned} \nabla U = &\left[\tfrac{\mu}{r^2} + \tfrac{k_{J2}}{r^4}(1 - 3\sin^2(i)\sin^2(\theta))\right]\boldsymbol{x}\\ &+ \left[\tfrac{k_{J2}}{r^4}\sin^2(i)\sin(2\theta)\right]\boldsymbol{y}\\ &+ \left[\tfrac{k_{J2}}{r^4}\sin^2(2i)\sin(\theta)\right]\boldsymbol{z}. \end{aligned} \tag{13}$$

Describing the secondary-body's position, velocity, and acceleration vectors in the LVLH frame is required to produce the gradient of the potential function applied to the secondary-body (Xu et al. 2012)

$$\boldsymbol{r} = r\boldsymbol{x}, \tag{14}$$

$$\frac{d}{dt}(\boldsymbol{r}) = \boldsymbol{V} = v_x\boldsymbol{x} + \frac{\boldsymbol{h}}{r}\boldsymbol{y}, \tag{15}$$

$$\frac{d^2}{dt^2}(\boldsymbol{r}) = \left(\frac{dv_x}{dt} - \frac{h^2}{r^3}\right)\boldsymbol{x} + \frac{1}{r}\frac{dh}{dt}\boldsymbol{y} + \omega_x\frac{h}{r}\boldsymbol{z}. \tag{16}$$

In the above equations, h is the angular momentum, which is defined as $h = |\boldsymbol{r} \times \frac{dr}{dt}|$. Establishing the relation between the unit vectors $\boldsymbol{r} = \boldsymbol{x}$, $\boldsymbol{r} = [r00]^T$, $\boldsymbol{r_3} = [x_3y_3z_3]^T$, and a combination of Equations (11) and (13), the potential function gradient acting on the secondary-body is encapsulated in the LVLH frame

$$\begin{aligned} \nabla W + \nabla U = &\left[\frac{\mu}{r^2} + \frac{k_{J2}}{r^4}(1 - 3\sin^2(i)\sin^2(\theta))\right.\\ &\left. + \left(\mu_3\left(\frac{1}{r_3^3} - \frac{1}{d_3^3}\right)x_3 - \frac{\mu_3}{d_3^3}r\right)\right]\boldsymbol{x}\\ &+ \left[\frac{k_{J2}}{r^4}\sin^2(i)\sin(2\theta) + \mu_3\left(\frac{1}{r_3^3} - \frac{1}{d_3^3}\right)y_3\right]\boldsymbol{y}\\ &+ \left[\frac{k_{J2}}{r^4}\sin(2i)\sin(\theta) + \mu_3\left(\frac{1}{r_3^3} - \frac{1}{d_3^3}\right)z_3\right]\boldsymbol{z} \end{aligned} \tag{17}$$

Now by taking on $\frac{d^2}{dt^2}(\boldsymbol{r}) = -(\nabla W + \nabla U)$ and by combining Equations (16) and (17), the secondary-body's motion with the primary-body's obliquity in the presence of third-body perturbations can be expressed as in Equations (18)–(23).

$$\frac{dr}{dt} = v_x. \tag{18}$$

$$\begin{aligned} \frac{dv_x}{dt} = &-\frac{\mu}{r^2} + \frac{h^2}{r^3} - \frac{k_{J2}}{r^4}(1 - 3\sin^2(i)\sin^2(\theta))\\ &+ \left(\mu_3\left(\tfrac{1}{r_3^3} - \tfrac{1}{d_3^3}\right)x_3 - \tfrac{\mu_3}{d_3^3}r\right). \end{aligned} \tag{19}$$

$$\frac{dh}{dt} = -\frac{k_{J2}}{r^3}\sin^2(i)\sin(2\theta) - r\mu_3\left(\frac{1}{r_3^3} - \frac{1}{d_3^3}\right)y_3. \tag{20}$$

$$\begin{aligned} \frac{d\theta}{dt} = &\cos(i)\sin(\theta)\frac{r}{h}\mu_3\left(\frac{1}{r_3^3} - \frac{1}{d_3^3}\right)z_3 + \frac{h}{r^2}\\ &+ \frac{k_{J2}}{hr^3}\cos^2(i)\sin^2(\theta). \end{aligned} \tag{21}$$

$$\begin{aligned} \frac{di}{dt} = &-\frac{k_{J2}}{hr^3}\sin(2i)\sin(2\theta)\\ &- \cos(\theta)\frac{r}{h}\mu_3\left(\frac{1}{r_3^3} - \frac{1}{d_3^3}\right)z_3. \end{aligned} \tag{22}$$

$$\begin{aligned} \frac{d\Omega}{dt} = &-\sin^2(\theta)\cos(i)\frac{k_{J2}}{hr^3}\frac{k_{J2}}{hr^3}\\ &- \frac{r}{h}\frac{\sin(\theta)}{\sin(i)}\mu_3\left(\frac{1}{r_3^3} - \tfrac{1}{d_3^3}\right)z_3. \end{aligned} \tag{23}$$

The non-simplified secondary-body motion equations are obtained with six hybrid orbital elements.

The secondary-body's motion can be evaluated using five equations, Equations (18)–(22), which are independent of Ω. Also, when utilizing these equations, the perturbing-body's inclination is considered to be important for long-time motion evaluation.

Moreover, the orbital rate ω_z is equal to (Wei et al. 2013)

$$\omega_z = \frac{h}{r^2}. \tag{24}$$

Also, the steering rate of the orbital plane will be extracted by applying Equations (16) and (17)

$$\omega_x = -\sin(2i)\sin(\theta)\frac{k_{J2}}{hr^3} - \frac{r}{h}\mu_3\left(\frac{1}{r_3^3} - \frac{1}{d_3^3}\right)z_3. \tag{25}$$

Now, employing (24), (25), and (18)–(20), the time derivative of the rotation components of the LVLH frame relative to the inertial coordinate can be derived as

$$\begin{aligned}\alpha_x &= \frac{d\omega_x}{dt} \\ &= \frac{k_{J2}}{r^3 h}\left(2i\cos(2i)\sin(\theta) + \frac{d\theta}{dt}\sin(2i)\cos(\theta)\right. \\ &\quad \left. - \frac{1}{h}\frac{dh}{dt} - \sin(2i)\sin(\theta)\frac{3v_x}{r}\right) \\ &\quad - \frac{k_{J2}}{hr^3}\sin(2i)\sin(\theta) - \frac{r}{h}\mu_3\left(\frac{1}{r}\frac{dr}{dt} - \frac{1}{h}\frac{dh}{dt}\right) \\ &\quad \left(\frac{1}{r_3^3} - \frac{1}{d_3^3}\right)z_3 - \frac{r}{h}\mu_3\left(\frac{1}{r_3^3} - \frac{1}{d_3^3}\right)\frac{dz_3}{dt} \\ &\quad + 3\frac{r}{h}\mu_3\left(\frac{1}{r_3^4}\frac{dr_3}{dt} - \frac{1}{d_3^4}\frac{dd_3}{dt}\right)z_3,\end{aligned} \tag{26}$$

$$\alpha_z = \frac{d\omega_z}{dt} = -\frac{2v_x h}{r^3} - \sin^2(i)\sin(2\theta)\frac{k_{J2}}{r^5} - \frac{1}{r}\mu\left(\frac{1}{r_3^3} - \frac{1}{d_3^3}\right)y_3, \tag{27}$$

where

$$\frac{d}{dt}(d_3) = \left[\left(\frac{dx_3}{dt} - \frac{dr}{dt}\right) + \frac{dy_3}{dt} + \frac{dz_3}{dt}\right]\Big/ d_3. \tag{28}$$

Applying Equations (18)–(23) requires knowing the displacement $[x_3 \quad y_3 \quad z_3]^T$ and velocity $\left[\frac{dx_3}{dt} \quad \frac{dy_3}{dt} \quad \frac{dz_3}{dt}\right]$ components of the third-body. These components are acquired by following the steps below:

1. The classical orbital elements of a third-body in an inclined elliptical orbit with a semimajor axis a_3, eccentricity e_3, inclination i_3, argument of perigee ω_3, argument of latitude θ_3 and RAAN Ω_3 are derived based on Keplerian motion.
2. The position and velocity vectors of the third-body are attained along the $\boldsymbol{p}$ (the apse line in the perifocal frame) and $\boldsymbol{q}$ (lies along the 90° true anomaly to $\boldsymbol{p}$) (Hintz 2015) by 1:

$$\bar{\boldsymbol{r}}_3 = \frac{h_3}{\mu_3}\frac{1}{1 + e_3\cos(f_3)}(\cos(f_3)\boldsymbol{p} + \sin(f_3)\boldsymbol{q}), \tag{29}$$

$$\dot{\bar{\boldsymbol{r}}}_3 = \bar{v}_3 = \frac{h_3}{\mu_3}[-\cos(f_3)\boldsymbol{p} + (e_3 + \cos(f_3))\boldsymbol{q}]. \tag{30}$$

3. The position and velocity vectors of the third-body in the inertial frame are obtained from the perifocal frame by:

$$Q_p^E = \begin{bmatrix} C_{\omega_3}C_{\Omega_3} - S_{\omega_3}C_{i_3}S_{\Omega_3} & -S_{\omega_3}C_{\Omega_3} - C_{\omega_3}C_{i_3}S_{\Omega_3} & S_{\omega_3}S_{\Omega_3} \\ C_{\omega_3}S_{\Omega_3} + S_{\omega_3}C_{i_3}C_{\Omega_3} & -S_{\omega_3}S_{\Omega_3} - C_{\omega_3}C_{i_3}C_{\Omega_3} & -S_{i_3}C_{\Omega_3} \\ S_{\omega_3}S_{i_3} & C_{\omega_3}S_{i_3} & C_{i_3} \end{bmatrix}, \tag{31}$$

where $S_* = \sin(*)$, $C_* = \cos(*)$.

$$\boldsymbol{r}_3^E = Q_p^E\bar{\boldsymbol{r}}_3. \tag{32}$$

$$\boldsymbol{v}_3^E = Q_p^E\bar{v}_3. \tag{33}$$

4. The position and velocity vectors of the third-body in the LVLH frame (located on the secondary-body) can be derived by

$$\Phi_E^L = \begin{bmatrix} C_\theta C_\Omega - S_\theta C_i S_\Omega & C_\theta C_\Omega + S_\theta C_i C_\Omega & S_\theta S_i \\ S_\theta C_\Omega - C_\theta S_i S_\Omega & -S_\theta S_\Omega - C_\theta C_i C_\Omega & C_\theta S_i \\ S_i S_\Omega & -S_i C_\Omega & C_i \end{bmatrix}, \tag{34}$$

$$\boldsymbol{r}_3 = \Phi_E^L\boldsymbol{r}_3^E = [x_3 \quad y_3 \quad z_3]^T, \tag{35}$$

$$\boldsymbol{v}_3 = \Phi_E^L\boldsymbol{v}_3^E = \left[\frac{dx_3}{dt} \quad \frac{dy_3}{dt} \quad \frac{dz_3}{dt}\right]. \tag{36}$$

3. Result Analysis

At first, some numerical simulations were done to demonstrate the proposed model's validity for secondary-body motion. The model presented by Liu et al. (2012) was employed to validate Equations (18)–(23). Subsequently, the outcomes of this model can be explored.

3.1. Validation

Contrary to some previous works (Castelli 2012; Mardling 2013; Sosnitskii 2014; Kholostova 2015; Rollin et al. 2016; Singh & Tyokyaa 2016; Topputo 2016), here, the perturbing-body's inclination is not taken as zero. No restrictions or simplifications have been invested when deriving the motion equations or simulations considering third-body effects. The motion of the secondary-body was compared with the results for the DA method using similar orbital parameters. Figure 2 illustrates the effect of primary-body obliquity and the

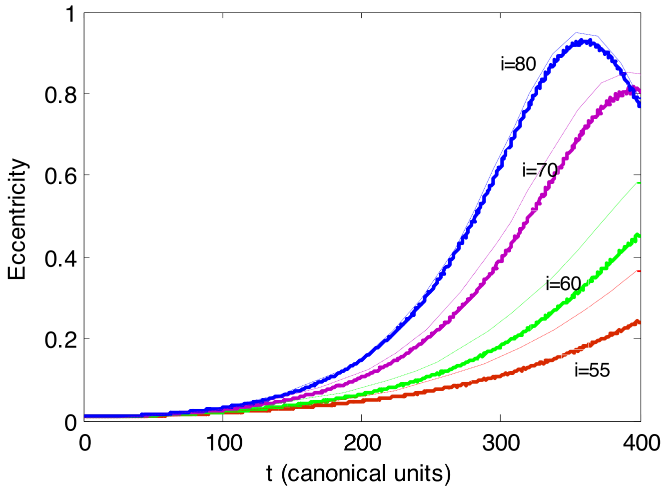

Figure 2. Variation of inclination in 400 canonical time units for various initial inclinations; double-averaged model (Liu et al. 2012) (dashed line), the proposed model (solid line).

difference between the DA and the proposed exact solution using Equations (18)–(23). The parameters used in Figure 2 are similar to those in Liu et al. (2012). In Figure 2 the eccentricity of the secondary-body is varied due to the effect of Kozai–Lidov oscillation. Both Kozai and Lidov found that the oscillation of a secondary-body's eccentricity and inclination is much longer than its orbital period (Naoz 2016). The parameters used in Figure 2 are similar to those in Liu et al. (2012).

The proposed model shows good accuracy and can be used to investigate the planetary orbiters problem further. Furthermore, Table 1 lists the DA's root mean square error (RMSE) and the proposed model for better comparison with a hierarchical three-body system. Here, the N-body (numerical integration of the N-body equations of motion) algorithm is employed as an accurate numerical method to show the error created by the DA and proposed models. The parameters chosen are $\frac{m_3}{M} = 10$, $\frac{a_3}{a} = 50$, $e_3 = 0.25$, $e = 0.2$, $\theta = 0$.

As expressed in Table 1, the proposed model is more accurate than the DA model, especially for orbits with high inclination. In the next section, results show that the DA's error is increased, and results become unreliable with increasing time. The DA approximation made simplifications to insert the gravity effect of the third-body in the motion equation of the secondary-body (quadrupole approximation) (de Almeida Prado & Vieira Neto 2006; de Almeida Prado 2003). Also, the DA model ignores the short-term oscillations, which cause an accumulation of errors in a long-term investigation (Ricker et al. 2015).

In former studies, the gravitational potential of a perturbing-body are expanded in terms of $(a/a_3)^n$. Most of them are expanded to the quadrupole ($n = 2$), which breaks down for

Table 1
Evaluation of RMSE for Double-average and Present Model Compared to N-body Algorithm for Different Values of Initial Inclination of Asteroid Orbiter

	Double-average Model		Present Model	
=-	Eccentricity	Inclination (deg)	Eccentricity	Inclination (deg)
$i_0 = 80$	0.021	2.54	0.007	0.37
$i_0 = 75$	0.025	3.04	0.009	0.42
$i_0 = 65$	0.031	3.65	0.009	0.46
$i_0 = 60$	0.039	4.37	0.010	0.50
$i_0 = 55$	0.049	5.05	0.011	0.51
$i_0 = 50$	0.063	5.59	0.011	0.53

prolonged moderately-hierarchical systems ($\frac{a_3}{a} \leqslant 100$). Some studies have expanded the potential gravity of the perturbing-body to octupole ($n = 3$) to prevent a significant change in the long-term evaluation results (Katz et al. 2011; Lithwick & Naoz 2011). The octupole level of approximation yields an interesting behavior even beyond the Kozai angles and is associated with high-order resonances that result in extremely large eccentricity peaks and flips. In addition, this approximation is useful in understanding a general hierarchical system and the Kozai–Lidov mechanism (Naoz 2016). However, some degree of simplification and ignoring of terms ($n = 4$, 5, ...) occurs in the octupole approximation. Thus, this approximation may consider some error in the triple system, and it is appropriate to propose a non-simplified method for this problem.

3.2. Third-body's Inclination and Eccentricity

In this section, some results are acquired to show the third-body's inclination and eccentricity effects on the long-term investigation of the orbital characteristics of the secondary-body in a moderately-hierarchical triple system. Furthermore, the outcomes illustrate the significance of the effects of ignorance of the primary-body's obliquity in previous work due to simplification. Likewise, evaluating the impact of secondary-body eccentricity, inclination, and RAAN is also essential. A generalized three-body system is examined to investigate the effect of third-body orbital elements further.

In this work, the time unit equals the period of the third-body orbiting the primary-body and initial conditions of the secondary-body are assumed as $\omega = \theta = \Omega = 0$, $i_0 = 60°$ and $a = 8R$ (R is the primary-body's radius). The results are derived from highly-elliptic orbits by various eccentricities of the secondary-body orbit ($e = 0.0$, 0.2, 0.5). Moreover, it is supposed that the orbital elements of the third-body are: $i_3 = 10°$, $\omega_3 = \theta_3 = \Omega_3 = 0$, $a_3 = 250a$, and eccentricity is assumed to be in the interval $0 \leqslant e_3 \leqslant 0.4$. According to the assumptions, the effect of third-body eccentricity on the inner binary orbit can then be investigated.

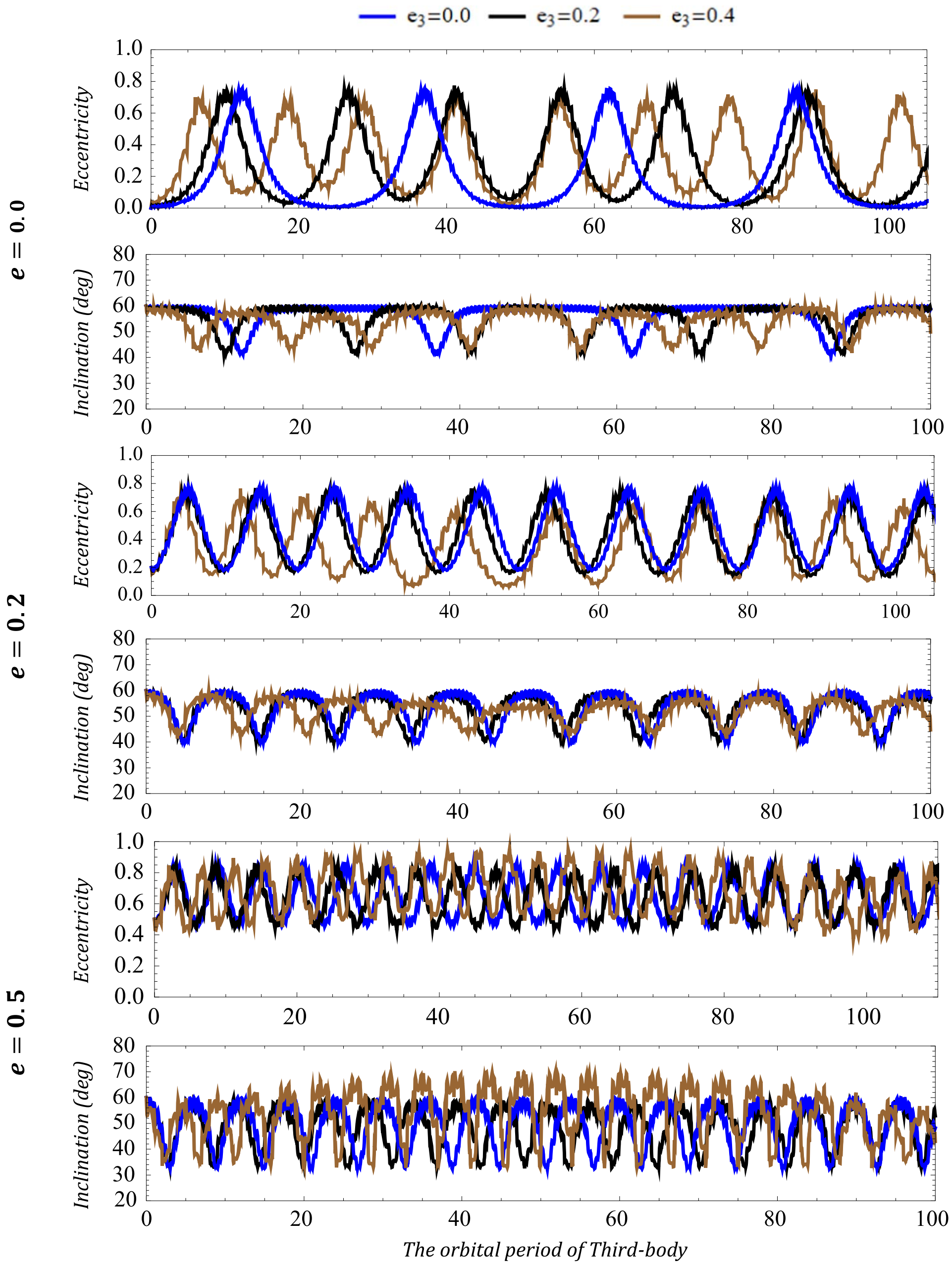

Figure 3. Variations of inclination and eccentricity for secondary-body orbit, on the orbital period of the third-body for different eccentricities. The initial conditions of the secondary-body are assumed as $\omega = \theta = \Omega = 0$, $i_0 = 60°$ and $a = 8R$, and those for the third-body are: $i_3 = 10°$, $\omega_3 = \theta_3 = \Omega_3 = 0$, $a_3 = 250a$.

Figure 3 illustrates the third-body's eccentricity effect on the alteration of the orbital elements of the secondary-body in a prolonged mission. Eccentricity variation of the third-body's orbit does not cause significant changes in the amplitude of inclination or eccentricity. In this case the secondary-body inclination and eccentricity have some large variation, but in some cases the raising of eccentricity can lead to instability of the three bodies over time. This oscillation of inclination is apparent in the investigation of two planet candidates KOI-275.01 and KOI 275.02. The two left panels present the evolutions of their orbital inclinations relative to the orbital plane of the proposed stellar companion and their mutual orbital inclination (Wang et al. 2014). This study shows a large variation in inclination.

Furthermore, the variation of the RAAN of a secondary-body's orbit is illustrated in Figure 4. Variation in the RAAN gets faster by increasing the eccentricity of the third-body.

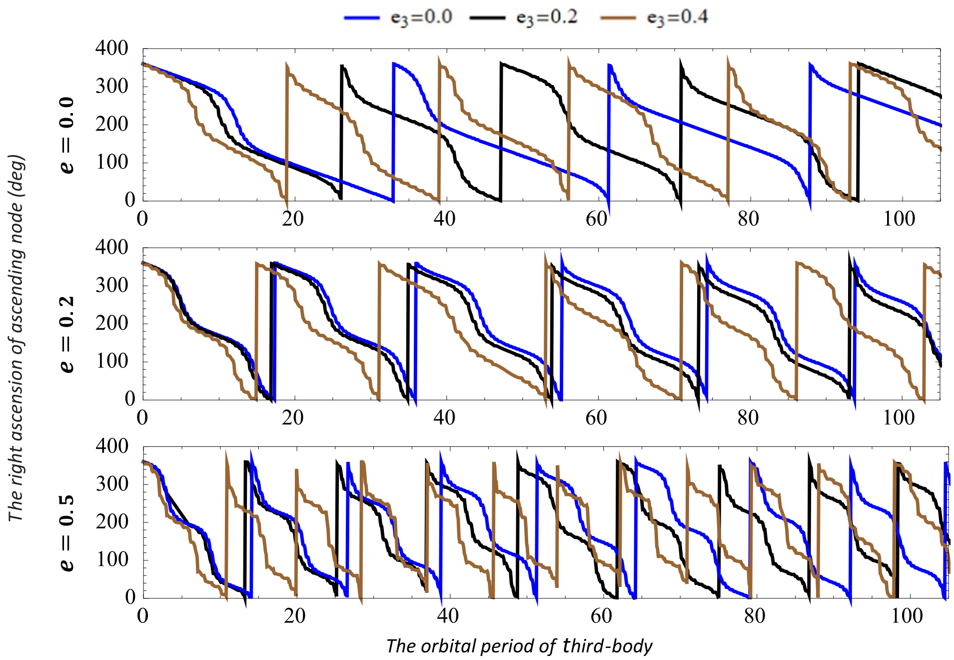

Figure 4. Evaluation of the RAAN of the secondary-body in the presence of a third-body with different eccentricity. The initial conditions of the secondary-body are assumed as $\omega = \theta = \Omega = 0$, $i_0 = 60°$, $a = 8R$, and those for the third-body are: $i_3 = 10°$, $\omega_3 = \theta_3 = \Omega_3 = 0$, $a_3 = 250a$.

In the following, the importance of the inclination of the third-body and primary-body's obliquity is more significant when the secondary-body has an eccentric orbit, as seen in some exoplanets such as 30 Arietis Bb. The new best-fit Keplerian orbital solution, along with the fit residuals, was provided (Kane et al. 2015). The parameters include eccentricity, periastron argument, orbital period, time of periastron passage, periastron argument, radial velocity (RV) semi-amplitude, semimajor axis, minimum planet mass, and the RV linear trend (Guenther et al. 2009). A generalized three-body system was considered to demonstrate the importance of obliquity and a high-order perturbing force on a prolonged mission for further investigation. In this example, the eccentricity of the perturbing-body is $e_3 = 0.2$, and obliquity is assumed to be in the interval $0° \leqslant i_3 \leqslant 100°$. Also, mass and semimajor axis ratios equal 100 and 250, respectively. The initial values of inclination and eccentricity are 70° and 0.2 for a secondary-body with different initial inclinations ($i = 20°$, 50°, 80°) and $\omega = \Omega = 0$.

Next, an evaluation of the inclination and eccentricity of the secondary-body's orbit is displayed in Figure 5 by employing Equations (18)–(23). In previous works that ignore the primary-body's obliquity, the $X - Y$ plane (in an inertial frame) is considered the third-body's orbital plane instead of the equatorial plane of the primary-body. In this sense, the inclination of the third-body is assumed to be zero (Bello & Singh 2015). This simplification causes significant errors in the prolonged evaluation of the non-planar three-body system, specifically in the case of a massive perturbing-body.

Furthermore, previous works (Broucke 2003; Domingos et al. 2014) have reported that if the secondary-body's orbital inclination is lower than the critical value ($i = 39.°2$), its eccentricity does not vary remarkably in the presence of the perturber (third-body). On the contrary, when the secondary-body's inclination is above the critical inclination, the orbit becomes very elliptic over time, as affirmed in Figure 5. When ignoring the primary-body obliquity, the critical inclination is about 39.°2 (de Almeida Prado 2003).

As demonstrated in Figure 5, with an increase in the third-body, the variation of the eccentricity of the secondary-body occurs in a wider range, unless $|i - i'|$ is lower than the critical inclination of 39.°2. Also, the inclination of the secondary-body around the retrograde third-body (inclination greater than 90°, red lines) changes in the opposite direction of the prograde third-body (inclination less than 90°, black and blue lines). The importance of obliquity or inclination of the third-body is evident in these simulations. Moreover, in Figure 5, Kozai–Lidov oscillation is present which leads to large variations between the eccentricity and inclination of the secondary-body's orbit.

Figure 6 illustrates the effect of the semimajor axis ratio of a third-body's orbit on secondary-body eccentricity and inclination. It is demonstrated that the semimajor axis ratio $\frac{a_3}{a}$ is the

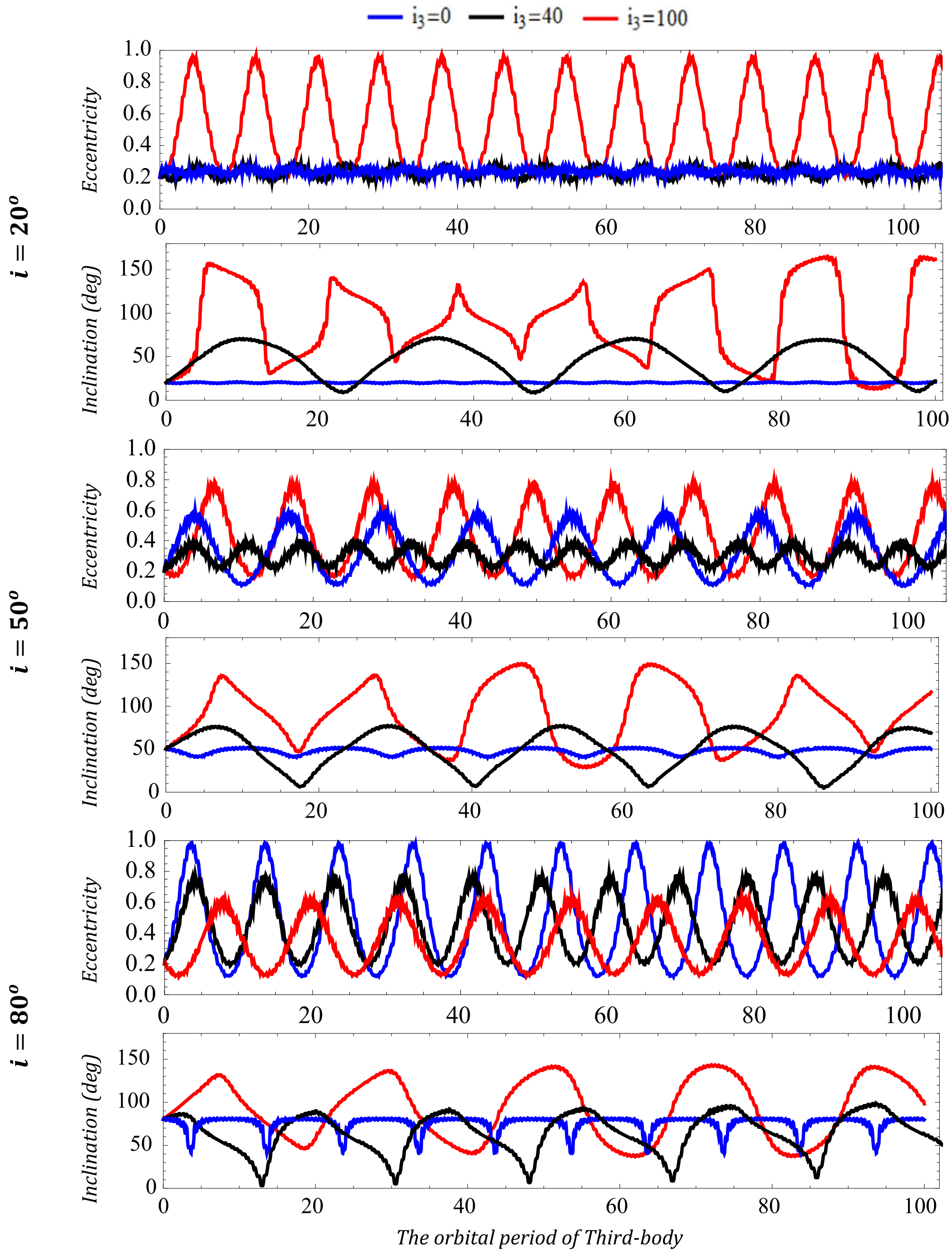

Figure 5. Changes in inclination and eccentricity of the secondary-body under the influence of a third-body with different inclinations. The initial conditions of the secondary-body are assumed to be $\omega = \theta = \Omega = 0$, $e = 0.2$, and those for the third-body are: $e = 0.2$, $\omega_3 = \theta_3 = \Omega_3 = 0$, $a_3 = 100a$.

important factor affecting the motion of the secondary-body. By decreasing the semimajor axis ratio $\frac{a_3}{a}$, the disturbing force of the third-body becomes more influential, and the importance of the primary-body's obliquity (third-body's inclination) is evident (see the case of $\frac{a_3}{a} = 20$). In this case, the secondary-body motion becomes unstable and escapes from the primary-body orbit. Also, with the third-body moving away, slower changes occur in the orbital elements of the secondary-body.

It should be noted these results are also under the influence of the mass ratio $(\frac{m_3}{M})$, assuming that this value is constant and equal to 100 in the above simulations. For this simulation, a generalized three-body system with various values of a_3/a is

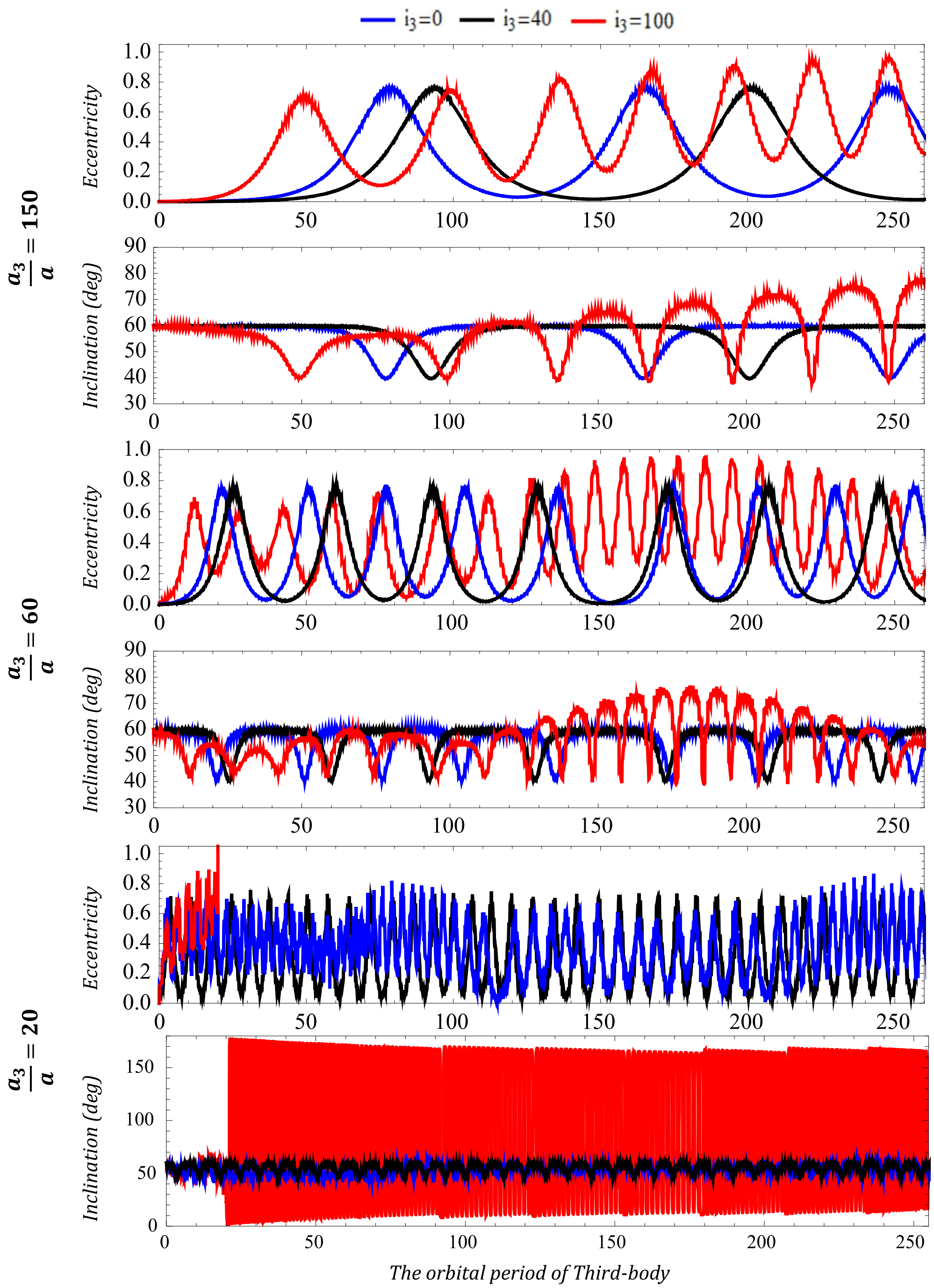

Figure 6. Variations of inclination and eccentricity over 250 periods of the third-body orbit for different semimajor axis ratios. The initial conditions of the secondary-body are assumed as $\omega = \theta = \Omega = 0$, $e = 0.2$, $i = 60°$, and for the third-body they are: $e = 0$, $\omega_3 = \theta_3 = \Omega_3 = 0$, $\frac{m_3}{M} = 100$.

examined. The initial conditions of the secondary-body are ($e = 0.2$), $\omega = \Omega = 0$ and $i = 60°$ and the third-body is moving in a circular orbit.

Figure 7 illustrates the effect of mass ratio on inclination of the secondary-body's orbit. It is shown that the mass ratio of ($\frac{m'}{M}$) and semimajor axis ratio ($\frac{a'}{a}$) are the important factors affecting the accuracy of the results. By increasing $\frac{m'}{M}$, the disturbing force of the third-body becomes more influential, and the importance of the primary-body obliquity is evident.

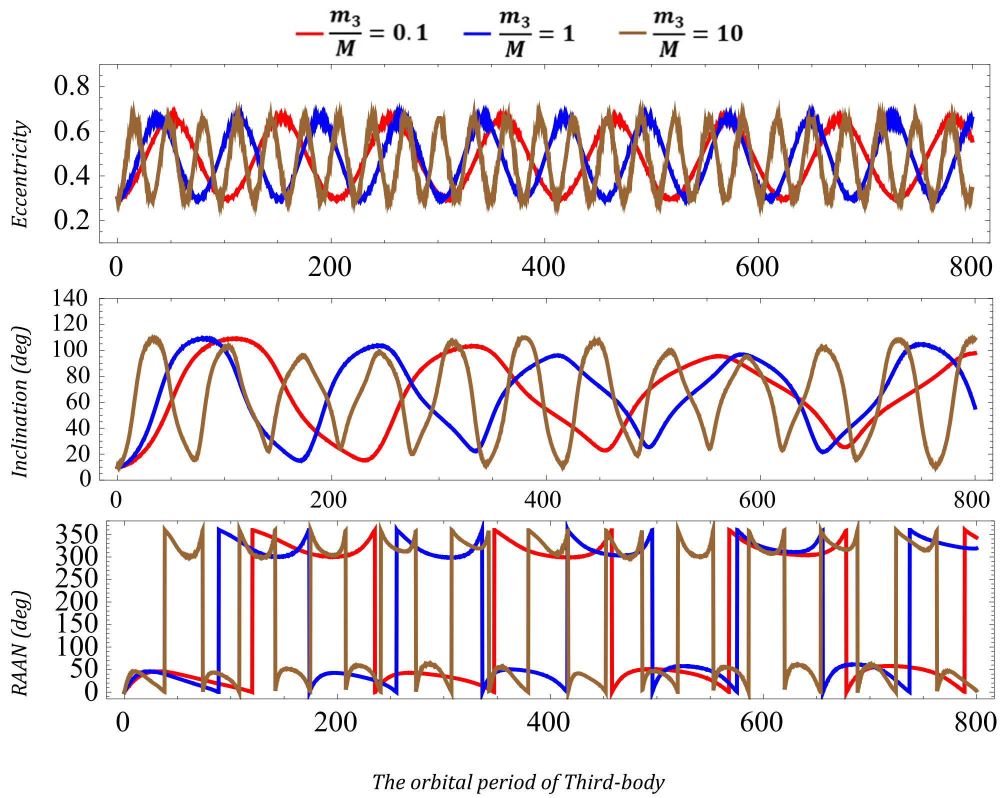

Figure 7. Variations of inclination and eccentricity over 800 periods of the third-body orbit for different mass ratios. The initial conditions of the secondary-body are assumed as $\omega = \theta = \Omega = 0$, $e = 0.3$, $i = 60°$, and for the third-body they are: $e = 0.2$, $i = 60°$, $\omega_3 = \theta_3 = \Omega_3 = 0$, $a_3 = 40a$.

4. Conclusions

This paper proposes a new non-simplified model for investigating problems in long-term missions. This model can be applied to all eccentricities, inclinations, and massive perturbers in a moderately-hierarchical system with wide application in astrophysics. Several previous works have ignored the effects of the obliquity of the primary-body on prolonged evaluation. That way, previously, the $X - Y$ plane of inertial coordinate (placed on the centroid of the primary-body) was assumed as the third-body's orbital plane (for simplification) instead of the equatorial plane of the primary-body. Here, it is shown that ignorance of obliquity leads to a remarkable error in prolonged evaluation. The proposed model shows good agreement compared to the *N*-body numerical integration algorithm, but the error in DA approximation increases over time. For a more detailed examination of the third-body effect on the prolonged motion of the secondary-body, a general three-body system has been introduced to investigate the perturbing effect of eccentricity and inclination and Kozai–Lidov oscillation. Thus, consideration of the obliquity of the primary-body is required in the long-term evaluation of three-body systems. Finally, the effect of the semimajor axis ratio is studied and shown on the motion of the secondary-body.

References

Abbasali, E., Kosari, A., & Bakhtiari, M. 2021, AdSpR, 68, 4379
Abouelmagd, E. I., Guirao, J. L. G., & Pal, A. K. 2020, NewA, 75, 101319
Bakhtiari, M., Daneshjou, K., & Abbasali, E. 2017a, Ap&SS, 362, 1
Bakhtiari, M., Daneshjou, K., & Fakoor, M. 2017b, RAA, 17, 039
Bakhtiari, M., Daneshjou, K., & Fakoor, M. 2017c, Aerosp. Sci. Technol., 70, 286
Bello, N., & Singh, J. 2015, AdAst, 2015
Broucke, R. A. 2003, JGCD, 26, 615
Carvalho, J. P. D. S., de Moraes, R. V., & Prado, A. F. B. D. A. 2011, Mathematical Problems in Engineering, 2011, 187478
Castelli, R. 2012, CNSNS, 17, 804
de Almeida Prado, A. F. B. 2003, JGCD, 26, 33
de Almeida Prado, A. F. B., & Vieira Neto, E. 2006, JAnSc, 54, 567
Domingos, R., Prado, A., & Gomes, V. 2014, Mathematical Problems in Engineering, 2014, 359845
Domingos, R. D. C., De Almeida Prado, A., & Vilhena De Moraes, R. 2015, JCoAM, 34, 507
Gomes, V. M., & de Cássia Domingos, R. 2016, JCoAM, 35, 653
Grishin, E., Perets, H. B., Zenati, Y., & Michaely, E. 2017, MNRAS, 466, 276
Guenther, E., Hartmann, M., Esposito, M., et al. 2009, A&A, 507, 1659
Han, E., Wang, S. X., Wright, J. T., et al. 2014, PASP, 126, 827
Ito, T. 2016, AdAst, 2016
Kane, S. R., Barclay, T., Hartmann, M., et al. 2015, ApJ, 815, 32
Katz, B., Dong, S., & Malhotra, R. 2011, PhRvL, 107, 181101
Kechichian, J. A. 1998, JAnSc, 46, 25
Kholostova, O. 2015, IJNLM, 73, 64
Lara, M. 2022, AcAau, 195, 596
Lithwick, Y., & Naoz, S. 2011, ApJ, 742, 94
Liu, X., Baoyin, H., & Ma, X. 2012, Ap&SS, 339, 295

Luo, L., Katz, B., & Dong, S. 2016, MNRAS, 458, 3060
Mardling, R. A. 2013, MNRAS, 435, 2187
Naoz, S. 2016, ARA&A, 54, 441
Neishtadt, A., Sheng, K., & Sidorenko, V. 2018, arXiv:1803.08847
Neishtadt, A., Sheng, K., & Sidorenko, V. 2021, CeMDA, 133, 1
Nie, T., & Gurfil, P. 2021, CeMDA, 133, 1
Ricker, G. R., Winn, J. N., Vanderspek, R., et al. 2015, JATIS, 1, 014003
Rollin, G., Lages, J., & Shepelyansky, D. 2016, NewA, 47, 97
Saeed, T., & Zotos, E. E. 2021, ResPh, 23, 103990
Singh, J., & Tyokyaa, R. K. 2016, EPJP, 131, 1
Sosnitskii, S. P. 2014, IJNLM, 67, 34
Topputo, F. 2016, CNSNS, 32, 89
Wang, J., Xie, J.-W., Barclay, T., & Fischer, D. A. 2014, ApJ, 783, 4
Wang, S.-C., Wu, X., & Liu, F.-Y. 2016, MNRAS, 463, 1352
Wei, C., Park, S.-Y., & Park, C. 2013, IJNLM, 55, 55
Xu, G., & Wang, D. 2008, JGCD, 31, 1521
Xu, G., Xiang, F., & Chen, Y. 2012, in 24th Chinese Control and Decision Conference (CCDC) (IEEE), 3676